

## RESEARCH ARTICLE

## Skeletal muscle shape influences joint torque exertion through the mechanical advantages

Jun Umehara,<sup>1,2</sup> Masashi Taniguchi,<sup>2</sup> Masahide Yagi,<sup>1,2</sup> Ganping Li,<sup>3</sup> Mazen Soufi,<sup>3</sup> Yoshito Otake,<sup>3</sup> Yoshinobu Sato,<sup>3</sup> Yoshihiro Fukumoto,<sup>1,2</sup> Momoko Yamagata,<sup>1,2</sup> Ryusuke Nakai,<sup>4</sup> and Noriaki Ichihashi<sup>1,2</sup>

<sup>1</sup>Faculty of Rehabilitation, Kansai Medical University, Hirakata, Japan; <sup>2</sup>Human Health Sciences, Graduate School of Medicine, Kyoto University, Kyoto, Japan; <sup>3</sup>Division of Information Science, Graduate School of Science and Technology, Nara Institute of Science and Technology, Ikoma, Japan; and <sup>4</sup>Institute for the Future of Human Society, Kyoto University, Kyoto, Japan

## Abstract

Skeletal muscle morphology is linked to its function. Extensive literature demonstrates that muscle volume is crucial for determining joint torque exertion, a primary function of muscle. However, whether muscle shape also influences torque exertion capacity remains unclear. This study illustrates that the three-dimensional shape of muscles independently determines joint torque exertion, irrespective of muscle volume, using a statistical shape model designed to quantify muscle shape features. The statistical shape model was developed from magnetic resonance images of the quadriceps femoris muscles in 33 healthy young adults (26 ± 5 yr; 18 males). We investigated the association between the shape components of each quadriceps femoris head and isometric knee extensor torque. The findings reveal that the mediolateral curvatures of the rectus femoris ( $R^2 = 0.60$ ) and the bulging in the distal region of the vastus medialis ( $R^2 = 0.65$ ) were associated with increased knee extensor torque despite muscle volumes. Moreover, the rectus femoris and vastus medialis shapes were correlated with the medial-directed line-of-action ( $r = -0.42$  and  $\rho = -0.36$ ). The vastus medialis shape was correlated with the moment arm of the patellar lateral spin ( $\rho = 0.45$ ). Therefore, the three-dimensional muscle shape determines the joint torque exertion by forming the mechanical advantages that balance the force/torque output optimally. Our findings demonstrate that muscle shape is crucial in the mechanical output of skeletal muscle and provides a framework for enhancing the understanding of muscle morphology and its functionality.

**NEW & NOTEWORTHY** Here, we developed a statistical shape model, a geometric model that can quantify muscle morphology, particularly the quadriceps femoris muscle, to determine the influence of three-dimensional muscle shape on its force-generating capacity in young adults. The results revealed that curvature of the rectus femoris and bulging of vastus medialis were determinants of isometric knee extension strength, coupled with their muscle volumes. This morphological functionality relies on the critical relationship between muscle shape and mechanical advantage.

*biomechanics; morphology; muscle function; statistical shape model*

## INTRODUCTION

Morphology of all the biological tissues is closely linked to function, and skeletal muscle is no exception. The primary function of skeletal muscle is to generate force and exert joint torque by leveraging the moment arm. Although the muscle force is predominantly determined by functional cross-sectional area (1), the final mechanical output, joint torque, is substantially governed by the muscle volume (2–4). For instance, Fukunaga et al. (5) observed the muscle volume of elbow flexor and extensor muscles using magnetic resonance imaging (MRI) and its relationship to the maximum voluntary isometric torque of elbow flexion and extension, finding a significant correlation between muscle volume and joint torque. Blazevich et al. (6) described the muscle volume of the vastus

lateralis (VL) as the best predictor of maximum isometric knee extensor torque, even when considering other morphological factors such as anatomical and physiological cross-sectional areas (ACSA and PCSA, respectively), fascicle length, and moment arm.

Although the muscle volume–joint torque relationship has been established, the joint torque cannot be fully predicted using only the muscle volume. Previous studies noted non-negligible errors in explaining joint torque by muscle volume (2–6), suggesting that other morphological factors should be considered in joint torque estimation when assuming volume as a proxy representing PCSA and moment arm (5) and minimal influence from neural factors (i.e., the muscle is fully activated). One potential factor is the three-dimensional (3-D) muscle shape. The 3-D muscle shape refers to a morphological



characteristic that reflects the 3-D nature of the muscle and its packing mechanism within the musculoskeletal system. The muscle shape is significant to function in terms of regional volume/area distribution and architectural gearing. For instance, nonuniform distributions of muscle volume between regions adaptively occurred in sprinters, attributable to torque generation and sprint performance (7). The inhomogeneous distribution of hypertrophy was induced by two different trainings (concentric and eccentric trainings), indicating the relationship between morphological adaptation and contractile behavior (8). In dynamic contraction, muscle gearing, the ratio of muscle fascicle shortening velocity to whole-muscle velocity (9), indicates the effect of muscle shape change on the mechanical output of muscle/contractile force (10–12).

Despite its asserted importance (13), direct investigations into 3-D muscle shape have been scarce. Previous studies mentioned above have evaluated muscle volume, area, and length but not quantified muscle shape directly, leaving the relationship between 3-D muscle shape and function largely unexplored. This gap may stem from the challenges in quantifying the complex 3-D shape of muscles. The current study addresses this issue through statistical shape modeling (14, 15), a population-based geometric model that describes a group of semantically similar individual shapes as a mean shape and variations representing distinct shape features. Statistical shape modeling has been applied in diverse fields including 3-D geometry reconstruction (16), automatic image segmentation (17), disease characterization/classification (18, 19), and personalized musculoskeletal modeling (20, 21). However, its use in exploring muscle function has been limited. Recent applications of statistical shape modeling have explored the morphological features of the soleus muscle in cerebral palsy (22) and classified hamstring morphology between rugby players and sprinters (23), but not its functional role.

In this study, we aimed to determine whether the 3-D muscle shape influences joint torque exertion. We constructed a statistical shape model from MRI images of the quadriceps femoris muscle, a common experimental muscle, and investigated the relationship between the muscle shape of the quadriceps femoris and isometric knee extensor torque. Building on previous studies on muscle volume as the predictor with non-negligible error (5, 6), we hypothesized that not only muscle volume but also muscle shape determines joint torque exertion by influencing the muscle moment arm and line-of-action, which modulates muscle force output. This study provides new insights into the morphological functionality of muscle, specifically analyzing the effect of 3-D muscle shape on force generation. These findings apply to strength training and rehabilitation, particularly targeting regional hypertrophy to enhance physical ability and sports performance.

## MATERIALS AND METHODS

### Participants

Thirty-three healthy adults (age:  $26.1 \pm 4.8$  yr; height:  $165.6 \pm 6.6$  cm; body mass:  $57.2 \pm 7.1$  kg; 18 males) participated in this study. Inclusion criteria included no history of lower extremity surgery; no medical history of rheumatoid arthritis, orthopedic injuries, neurological disorders, or cognitive

dysfunction; and no general contraindications for MRI. The study protocol was approved by the Ethics Committee of Kyoto University Graduate School and Faculty of Medicine (R1746) and conducted in accordance with the Declaration of Helsinki. All participants provided written informed consent before participating in the experiment.

### Experimental Protocol

The methodological overview is presented in Fig. 1. The participants were asked to refrain from excessive exercise and intake since the day before. MRI measurements and muscle strength assessments were conducted for all participants. In the MRI scans, the quadriceps femoris muscles were labeled using automatic segmentation and 3-D surface mesh models were created. Following a series of image processing and dimensionality reduction steps, the statistical shape model was constructed. This model represented the muscle shape through the mean shape and variance of shape components for all participants. To assess the impact of muscle shape on strength exertion, a regression analysis was conducted between the shape components in the statistical shape model of the quadriceps muscles and the knee extension torque.

### Magnetic Resonance Imaging

Participants were scanned using a 3.0-T MRI system (MAGNETOM Verio; Siemens AG, Germany), as shown in Fig. 1A. T1-weighted images of the right lower extremity were captured using a body matrix coil and a spine coil with the following multislice sequence parameters: acquisition plane was axial, field of view was  $320 \text{ mm} \times 240 \text{ mm}$ , slice thickness was 4 mm, resolution was  $0.5 \times 0.5 \times 4 \text{ mm}$ , repetition time (TR) was 2,820 ms, echo time (TE) was 16 ms, flip angle was  $129^\circ$ , and the interslice gap was 0 mm. Before the scans, three reflective markers, which are fat-embedded non-magnetic capsules, were attached to the right thigh at 25%, 50%, and 75% distances from the anterior superior iliac spine to the patella for subsequent image processing. After resting in a supine position for 15 min, the scanning was repeated three times by moving the MRI table to cover the entire target region, defined from the proximal part of the pelvis to the distal part of the right thigh. The center of the image was positioned at the femur head, the midpoint of the thigh, and the superior border of the patella in each scan. During the scanning, participants lay supine on the MRI table with their legs in a neutral position and their knee joints in full extension, secured with a wooden base to prevent postural changes, and were instructed to relax to avoid muscle deformation due to any contractions, thus maintaining the muscle's natural shape.

### Image Processing

The MRI images, divided into three sections, were rigidly stitched based on the reflective markers attached to the thigh, resulting in a reconstructed MRI image capturing the entire thigh. In these images, the heads of the quadriceps femoris muscle—rectus femoris (RF), vastus lateralis (VL), medialis (VM), and intermedius (VI)—were annotated using automatic segmentation employing a U-net-based Bayesian active learning framework (24) (Fig. 1B). This musculoskeletal segmentation method integrates density and diversity

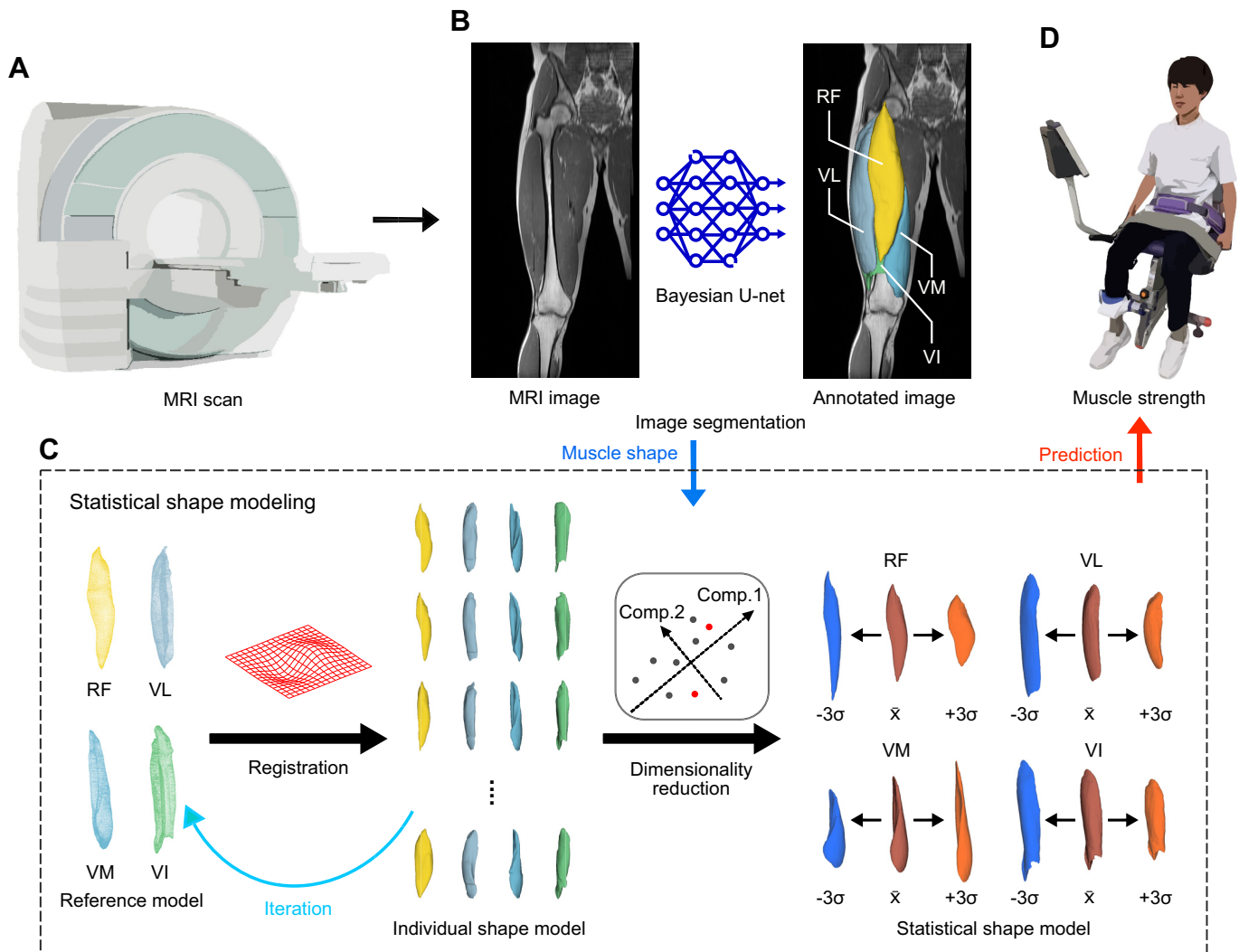


**Figure 1.** Methodological overview. *A*: image scan using the magnetic resonance imaging (MRI) system. *B*: image segmentation. The regions of quadriceps femoris muscles [i.e., rectus femoris (RF) and vastus lateralis (VL), medialis (VM), and intermedius (VI)] were annotated on the MRI image by the automatic segmentation using U-net-based Bayesian active learning framework. The MRI image and annotated image are used as input and output data, respectively. *C*: the series of procedures for the statistical shape modeling. A reference model was deformed to the individual shape models using rigid and nonrigid registrations iteratively for taking shape correspondence across individuals. Then, the dimensionality reduction was performed on the shape-corresponded individual models using the partial least square regression which described the shape variation into a small number of shape components, resulting in the statistical shape model where the variety of muscle shape was allowed to be represented by the mean shape ( $\bar{x}$ ) and its variance ( $\sigma$ ). Here, for representatives of shape variations, the mean shape and the shape with  $\pm 3$  standard deviations are shown. *D*: the muscle strength testing. The knee extensor torque was measured using dynamometer in sitting position. Regression model was created to predict the knee extensor torque from the muscle shape and volume.

criteria within a Bayesian active learning framework based on Bayesian U-net (25). The segmentation accuracy for the quadriceps femoris muscle on the MRI image was confirmed to be comparable with labels manually segmented by medical experts (24). After segmentation, all slices of the annotated image were visually inspected and manually refined as necessary. We refined 20 out of 33 subjects. Subsequently, the muscle volumes of the quadriceps femoris heads were calculated. In addition, the annotated image underwent filtering to fill small holes and smooth minor details using Gaussian filter (kernel size: 2 mm) and filling holes smoothing (kernel size: 3 mm) of the segmentation module in 3-D Slicer (v. 4.11; Harvard University, Boston, MA), preparing it for statistical shape modeling.

### Statistical Shape Modeling

The statistical shape model for the heads of the quadriceps femoris muscle was constructed through a three-step process that included shape representation, registration, and dimensionality reduction (Fig. 1C).

First, each head of the quadriceps femoris muscle annotated in the images was converted into a mesh model expressed as a dense surface point distribution model. The number of vertices to build the mesh models was  $32,674 \pm 5,943$  for the RF,  $73,313 \pm 11,770$  for the VL,  $53,645 \pm 8,057$  for the VM, and  $66,282 \pm 12,199$  for the VI. This conversion utilized a function from the segmentation module of 3-D slicer.

Second, registration was performed to establish shape correspondence among the mesh models of all participants. This process involved two steps. Initially, a model with median volume was selected as the initial reference model, aligned to the other models using rigid and affine transformations, and then further deformed to represent other shape models using B-spline transformation—a type of free-form deformation for exact warping of the model. A definitive reference model was created by averaging all mesh models. This registration process was repeated, replacing the initial reference with the definitive reference to minimize the influence of the initial reference model. Eventually, shape correspondence was based on the definitive reference model, with mesh models represented by 33,204 vertices for the RF, 75,192 for the VL, 49,428 for the VM, and 64,122 for the VI. Root-mean-square errors of these registrations were  $1.49 \pm 0.87$  mm for RF,  $1.56 \pm 0.70$  mm for VL,  $1.26 \pm 0.84$  mm for VM, and  $2.16 \pm 1.02$  mm for VI. The registrations were executed using the Image Registration Toolkit library (26).

Third, dimensionality reduction was conducted. The statistical shape model characterizes individual shapes by deviations from a mean shape. This mean shape is derived by averaging all individual models, whereas shape variation is determined by subtracting this mean shape from each individual shape. Subsequently, partial least squares regression (PLSR) was applied to the shape variations using the SIMPLS algorithm (27). PLSR, a supervised dimensionality reduction method, is capable of creating a new dimension by considering the covariance between the shape and a response variable. Similar to other dimensionality reduction techniques such as principal component analysis, PLSR is employed in the statistical shape model to achieve specific objectives (21) and its feasibility has been ensured (28). By defining knee extensor torque as the response variable, PLSR enables the description of shape variations through a limited number of shape components that are pertinent to muscle strength.

The model thus includes the mean shape and specific shape components for each head of the quadriceps femoris muscle. Before dimensionality reduction, the volume scaling method was used to scale the muscle volume of all individual models to the mean volume because this study focuses on muscle shape. Thus, the volume-scaled shapes were used for further analysis. All data processing was performed using MATLAB R2019b (MathWorks, Natick, MA).

### Mechanical Advantages

The muscle moment arm and line-of-action were determined for each head of the quadriceps femoris muscle based on the surface mesh model. Muscle centroids were identified at every 4 mm, equal to the slice thickness. A piecewise cubic spline was employed to calculate the muscle path (Fig. 2A). The muscle orientation was described by a series of tangent vectors along with the muscle path. The muscle orientation was determined by averaging one-third of the tangent vectors in the distal region (region close to the knee joint) and was represented by a unit vector in 3-D space. These methods were employed based on a similar approach used to estimate the 3-D orientation of muscle fascicles (29).

The line-of-action was expressed as direction cosine, the cosine of the angle between the 3-D unit vector of muscle orientation and the axis of the reference coordinate system (30). The reference coordinate system was defined as the patella (APPENDIX). The line-of-action was calculated in the transverse ( $\alpha$ ), sagittal ( $\beta$ ), and coronal ( $\gamma$ ) planes, respectively (31) (Fig. 2B). The moment arm about the patellofemoral joint was calculated using a triple scalar product (32). The muscle moment arm was computed by the scalar product of a unit vector specifying the direction of the axis of the joint coordinate system and the cross product of the unit vector of line-of-action and the vector from the joint center to any point along with the line-of-action. The quadriceps

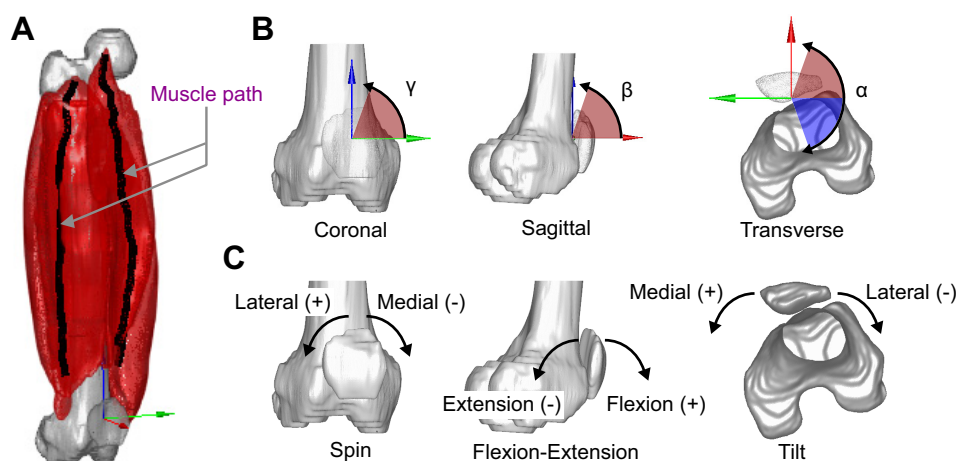


**Figure 2.** Muscle line-of-action and moment arm. **A:** schematic representation of the right thigh, depicting the quadriceps femoris muscle, femur, and patella. The black solid lines indicate the muscle path of the quadriceps femoris, calculated based on a series of muscle centroids using a piecewise cubic spline. The coordinate system is represented on the patella where the x-axis is the forward direction (red arrow), the y-axis is the medial direction (green arrow), and the z-axis is the upward direction (blue arrow). **B:** the line-of-action of the quadriceps muscle is expressed as a projection angle of the muscle path onto coronal ( $\gamma$ ), sagittal ( $\beta$ ), and transverse ( $\alpha$ ) planes. Because the line-of-action on the coronal and sagittal planes converge in the first and second quadrants, the line-of-action is the positive value (counter-clockwise). The line-of-action is positive (counter-clockwise) and negative (clockwise) values because the line-of-action on the transverse plane diverges on all quadrants. **C:** moment arm of the quadriceps femoris about the patellofemoral joint is represented. The moment arms are lateral (+) and medial (–) spin (left), flexion (+) and extension (–) (middle), and medial (+) and lateral (–) tilt (right).

moment arm was expressed about lateral-medial spin ( $x$ ), flexion-extension ( $y$ ), and medial-lateral tilt ( $z$ ) (33) (Fig. 2C).

**Muscle Strength**

The evaluation of knee extensor torque is depicted in Fig. 1D. Participants were seated on a chair equipped with a dynamometer (Isoforce GT-330; OG GIKEN Co., Okayama, Japan), with the knee joint positioned at 60° flexion. They exerted maximum knee extensor strength after participants were instructed to perform the knee extension as much as possible. The knee extensor strength during maximum voluntary contraction was measured twice, each for ~3 s, after familiarization sessions. The greater of the two force measurements was used, and the maximum torque (N·m) was calculated by multiplying the force (N) by the lever arm (m) of the dynamometer placed at 26 cm distal to the knee joint.

**Statistics**

A Jaccard similarity coefficient, which measures similarity ranging from 0 (no overlap) to 1 (identical objects), was used to assess shape variation. It indicates the similarity between

scaled individual shapes and their mean shape. The variance of the eigenvalues was calculated as a contribution rate, and this was used to determine the accumulated contribution rate of shape components, indicating the efficiency of the model in capturing essential shape variations by a limited number of shape components (34). The number of shape components to retrieve was determined by the adjusted Wold’s R criterion using leave-one-out cross validation. The adjusted Wold’s R was computed as a ratio of the successive predicted sum of squares, varying the number of shape components as the residual of the predicted dependent variable from the observed dependent one. The number of shape components was defined as the point where the adjusted Wold’s R first exceeds 0.95 (35). Shape components that met this criterion were utilized for further analyses regarding muscle shape and joint torque.

The normal distribution of the data was first verified using the Shapiro–Wilk test. To understand the extent to which muscle volume and shape influence muscle strength, the relationships between muscle volume, shape components, and knee extensor torque were evaluated using the Pearson/Spearman

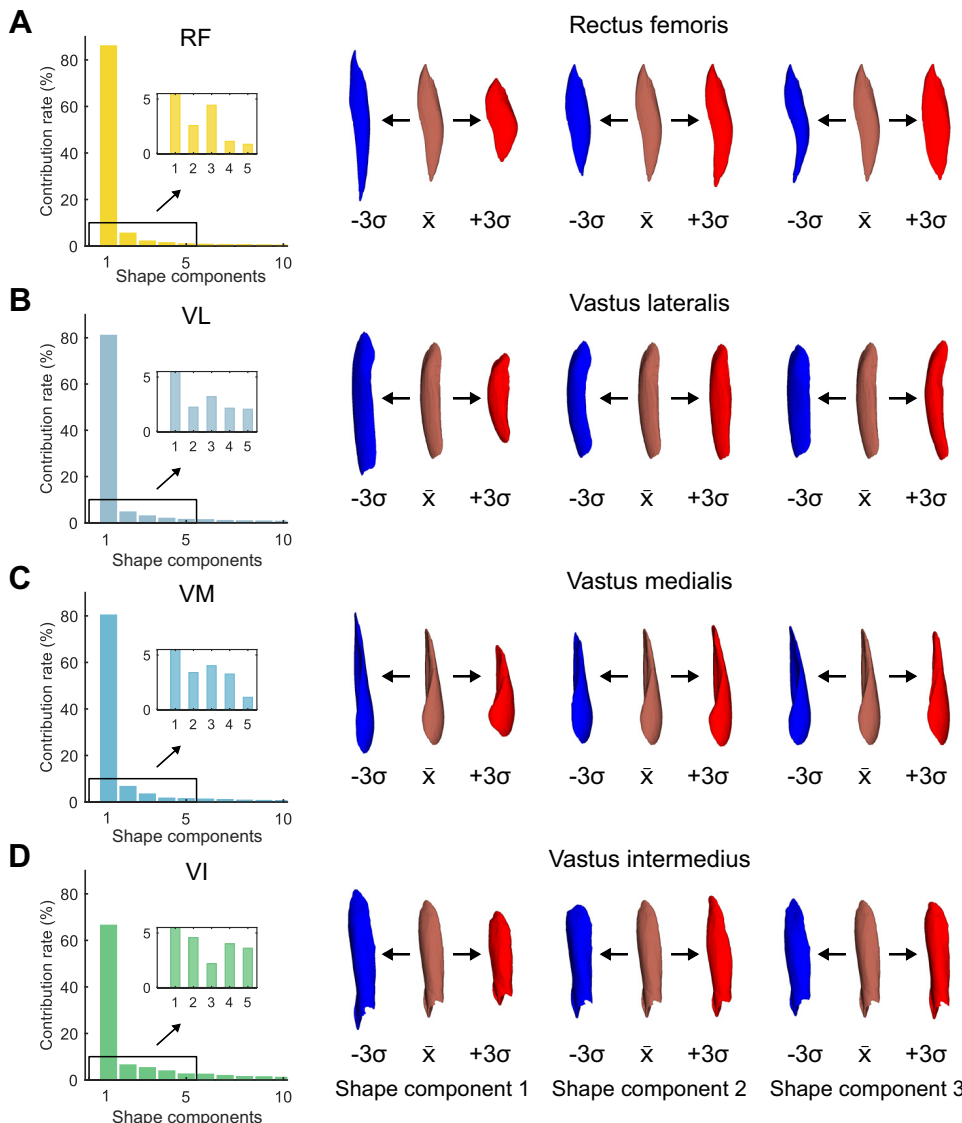


**Figure 3.** Statistical shape model of quadriceps femoris muscles. The bar graph shows the contribution rate against the number of shape component for the rectus femoris (RF), the vastus lateralis (VL), the vastus medialis (VM), and the vastus intermedius (VI). This figure exhibits the first ten shape components as representatives because the contribution rates are substantially small in subsequent components. The inset is the bar graph zoomed in the contribution rate of shape component from 1 to 5. The illustrations of muscle depict the muscle shapes characterized by the primary components (the first to third components). The shape variation is represented by the mean shape ( $\bar{x}$ ) and its  $\pm 3$  standard deviation ( $\sigma$ ) for the rectus femoris (A), the vastus lateralis (B), the vastus medialis (C), and the vastus intermedius (D). The muscle shapes in left, middle, right panels indicate the shapes based on the shape components 1–3.

correlation coefficient based on the normality. In addition, to ascertain the influence of muscle shape on joint torque, a multiple regression analysis was conducted. Based on our hypothesis that incorporating the muscle shape of the quadriceps femoris along with its muscle volume would better predict knee extensor torque, a multiple linear regression was implemented with the stepwise method. In this regression model, knee extensor torque was the dependent variable and muscle volume and shape components were the independent variable. In addition, the influence of sex was investigated by including it as an adjusted variable in the final regression model. Multicollinearity was confirmed using the variance inflation factors value. The moment arm and line-of-action were compared among muscles and axes/planes by two-way analysis and variance [Muscle (RF; VL; VM; VI) × Axis (spin; flexion-extension; tilt) or Muscle (RF; VL; VM; VI) × Plane (coronal; sagittal; transverse)]. Regarding the shape component identified as the significant independent variable in multiple regression, the Pearson/Spearman correlation coefficient was

computed with the muscle moment arm and line-of-action to confirm the association between muscle shape and mechanical advantages. All statistical analyses were performed using MATLAB R2019b (MathWorks, Natick, MA). The probability was adjusted using the Benjamini–Hochberg method because of the number of statistical tests performed in this study. An  $\alpha$  level of 0.05 was used for all the statistical analysis.

## RESULTS

### Shape Variation

Muscle shape variation was assessed using the Jaccard similarity coefficient (Supplemental Fig. S1A). The mean Jaccard similarity coefficients were  $0.71 \pm 0.07$  for the RF,  $0.70 \pm 0.07$  for the VL,  $0.74 \pm 0.06$  for the VM, and  $0.67 \pm 0.06$  for the VI muscles. Representative pairs of shape models are displayed in Supplemental Fig. S1B, illustrating that muscle shape varies even after scaling for muscle volume.

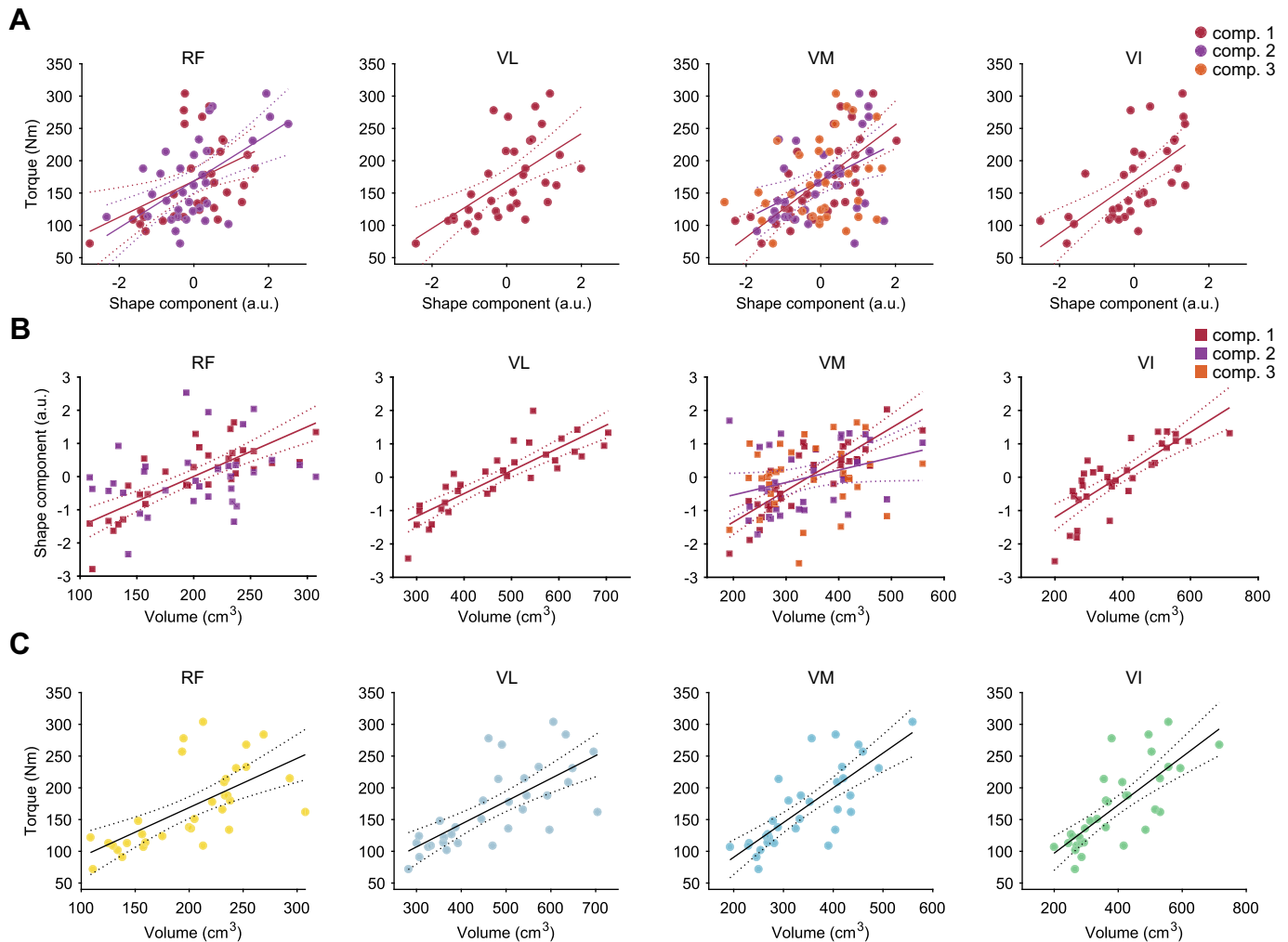


**Figure 4.** Correlations between shape components and muscle strength (A). Significant correlations were found between knee extensor torque and *shape component 1* of all muscles, *shape component 2* of the rectus femoris (RF) and the vastus medialis (VM), and *shape component 3* of the VM. Correlations between muscle volume and shape components (B). Significant correlations were found between muscle volume and *shape component 1* of all muscles and *shape component 2* of VM. Correlation between muscle volume and muscle strength (C). Significant correlations between knee extensor torque and muscle volume were found in all muscles. The dots show individual data. The solid and dashed lines indicate the least square regression line and 95% confidence bounds, respectively. a.u., arbitrary unit; VI, vastus intermedius; VL, vastus lateralis.

## Statistical Shape Model

The statistical shape model can describe the variation in muscle shape using a limited number of shape components. The relationship between the shape components is illustrated in the Supplemental Fig. S2. Figure 3 depicts the contribution rate of each shape component and illustrates the muscle shapes characterized by the primary components (the first to third components). *Component 1* accounted for a large amount of shape variation, which was 85.9%, 80.9%, 80.2%, and 66.3% of the variation of RF, VL, VM, and VI, respectively. The shapes' characteristics of *component 1* were size-related ones such as length and width/thickness for all muscles. *Component 2* accounted for 2.6%, 2.2%, 3.4%, and 4.6% of the variation of RF, VL, VM, and VI, respectively, which captures more complex shapes. For the RF muscle, curvature is a distinctive feature, occurring throughout the muscle in the anteroposterior and mediolateral directions. For the vasti muscles, the VL muscle displays curvature in the mediolateral direction, the VM muscle shows bulging at the distal part, and the VI muscle's proximal part becomes pointier. *Component 3* accounted for 4.4%, 3.2%, 4.0%, and 2.2% of the variation of RF, VL, VM, and VI, respectively. The RF and VL muscles primarily exhibit curvature similar to that seen with *component 2* but also show changes in width. For the VM muscle, the primary variation is in the ratio of width to thickness, whereas the VI muscle becomes overall rounder. Notably, the selection analysis of the number of components revealed that the first two components for the RF, the first component for the VL and VI, and the first three components for the VM met the threshold of the adjusted Wold's R and were deemed significant.

## Muscle Shape and Strength

The maximum knee extensor torque was measured at  $168.6 \pm 62.7$  N·m, with the Shapiro–Wilk test indicating non-normality. Correlation analysis assessed the relationship between the quadriceps femoris muscle shape and knee extensor torque (Fig. 4A). Significant correlations with knee extensor torque were observed in the first shape components of all muscles (RF:  $\rho = 0.50$ ,  $P = 0.003$ ,  $P_{\text{adj}} = 0.004$ ; VL:  $\rho = 0.64$ ,  $P < 0.001$ ,  $P_{\text{adj}} < 0.001$ ; VM:  $\rho = 0.73$ ,  $P < 0.001$ ,  $P_{\text{adj}} < 0.001$ ; VI:  $\rho = 0.71$ ,  $P < 0.001$ ,  $P_{\text{adj}} < 0.001$ ). Significant correlations were also found in the second components of RF ( $\rho = 0.46$ ,  $P = 0.007$ ,  $P_{\text{adj}} = 0.010$ ) and VM ( $\rho = 0.43$ ,  $P = 0.012$ ,  $P_{\text{adj}} = 0.016$ ) but not in the third component of VM ( $\rho = 0.25$ ,  $P = 0.162$ ,  $P_{\text{adj}} = 0.167$ ). The relationship between the muscle shape and its volume was evaluated (Fig. 4B). There were significant correlations between the first shape components and volumes in all muscles (RF:  $r = 0.79$ ,  $P < 0.001$ ,  $P_{\text{adj}} < 0.001$ ; VL:  $r = 0.85$ ,  $P < 0.001$ ,  $P_{\text{adj}} < 0.001$ ; VM:  $r = 0.84$ ,  $P < 0.001$ ,  $P_{\text{adj}} < 0.001$ ; VI:  $r = 0.80$ ,  $P < 0.001$ ,  $P_{\text{adj}} < 0.001$ ). The volume was significantly correlated with the second shape component in the VM ( $\rho = 0.37$ ,  $P = 0.037$ ,  $P_{\text{adj}} = 0.045$ ) but not with the second component of the RF ( $r = 0.26$ ,  $P = 0.147$ ,  $P_{\text{adj}} = 0.157$ ) and the third component of VM ( $r = 0.17$ ,  $P = 0.353$ ,  $P_{\text{adj}} = 0.353$ ). Ordinarily, significant relationships were confirmed between knee extensor torque and muscle volume for all muscles (RF:  $\rho = 0.73$ ,  $P < 0.001$ ,  $P_{\text{adj}} < 0.001$ ; VL:  $\rho = 0.76$ ,  $P < 0.001$ ,  $P_{\text{adj}} < 0.001$ ; VM:  $\rho = 0.82$ ,  $P < 0.001$ ,  $P_{\text{adj}} < 0.001$ ; VI:  $\rho = 0.79$ ,  $P < 0.001$ ,  $P_{\text{adj}} < 0.001$ ) (Fig. 4C).

Multiple linear regression analysis determined the role of muscle shape in knee extensor torque despite muscle volume (Table 1). For the VL and VI muscles, only muscle volume was identified as a significant independent variable (VL:  $R^2 = 0.51$ ,  $P < 0.001$ ,  $P_{\text{adj}} < 0.001$ ; VI:  $R^2 = 0.57$ ,  $P < 0.001$ ,  $P_{\text{adj}} < 0.001$ ), indicating that torque can be adequately predicted by muscle volume alone. However, for the RF and VM muscles, both muscle volumes and shapes were significant independent variables for torque. Notably, the second shape components of the RF and VM muscles were highlighted as significant (RF:  $R^2 = 0.60$ ,  $P < 0.001$ ,  $P_{\text{adj}} < 0.001$ ; VM:  $R^2 = 0.65$ ,  $P < 0.001$ ,  $P_{\text{adj}} < 0.001$ ) (Figs. 5A and 6A), suggesting that muscle shape contributes significantly to torque production, beyond muscle volume alone. The influence of sex on the relationship between joint torque and muscle volume and shape was little because sex was not a significant variable in the final regression model (Supplemental Document).

Figures 5B and 6B illustrate changes in muscle shape corresponding to the significant independent variables for knee extensor torque. For the RF muscle, pronounced changes occurred in the anterior-posterior and medial-lateral directions, where increased posterior and lateral curvatures of the proximal and distal regions correlated with higher torque (Fig. 5B). For the VM muscle, significant shape changes in the distal region, particularly greater bulging in distal region, were associated with increased knee extensor torque (Fig. 6B).

## Muscle Shape and Mechanical Advantages

The muscle moment arm and line-of-action are shown in Fig. 7. All quadriceps femoris muscles exhibited significant large moment arms for spin and flexion extension, which differed among muscles when compared with the tilt moment arm (Muscle  $\times$  Axis:  $F = 225.1$ ,  $P < 0.001$ ,  $P_{\text{adj}} < 0.001$ ; Muscle:  $F = 429.1$ ,  $P < 0.001$ ,  $P_{\text{adj}} < 0.001$ ; Axis:  $F = 350.1$ ,  $P < 0.001$ ,  $P_{\text{adj}} < 0.001$ ). Although the line-of-action of each muscle was diverse in the transverse plane, it did not vary among muscles in the coronal and sagittal planes where the lines of actions of all muscles

**Table 1.** Linear regression model for the joint torque exertion

Muscle	Independent Variables	B	$\beta$	P Value
RF	Volume	0.64	0.54	<0.001
	Shape component 1	4.46	0.07	0.727
	Shape component 2	27.51	0.44	<0.001
VL	Volume	0.36	0.72	<0.001
	Shape component 1	-6.39	-0.10	0.680
VM	Volume	0.49	0.70	<0.001
	Shape component 2	14.77	0.24	0.048
	Shape component 3	11.42	0.18	0.097
VI	Volume	0.38	0.76	<0.001
	Shape component 1	7.35	0.12	0.556

Multiple regression analysis with the stepwise method was performed by specifying knee extensor torque as a dependent variable and muscle volume and shape components as independent variables. The variance inflation factor (VIF) value was calculated to confirm the multicollinearity effect on the prediction models. The VIF value of the first shape component of VM muscle was relatively high (VIF = 5.34). Thus, this independent variable was eliminated in the final model.  $\beta$ , standardized partial regression coefficient; B, partial regression coefficient; RF, rectus femoris; VI, vastus intermedius; VL, vastus lateralis; VM, vastus medialis.

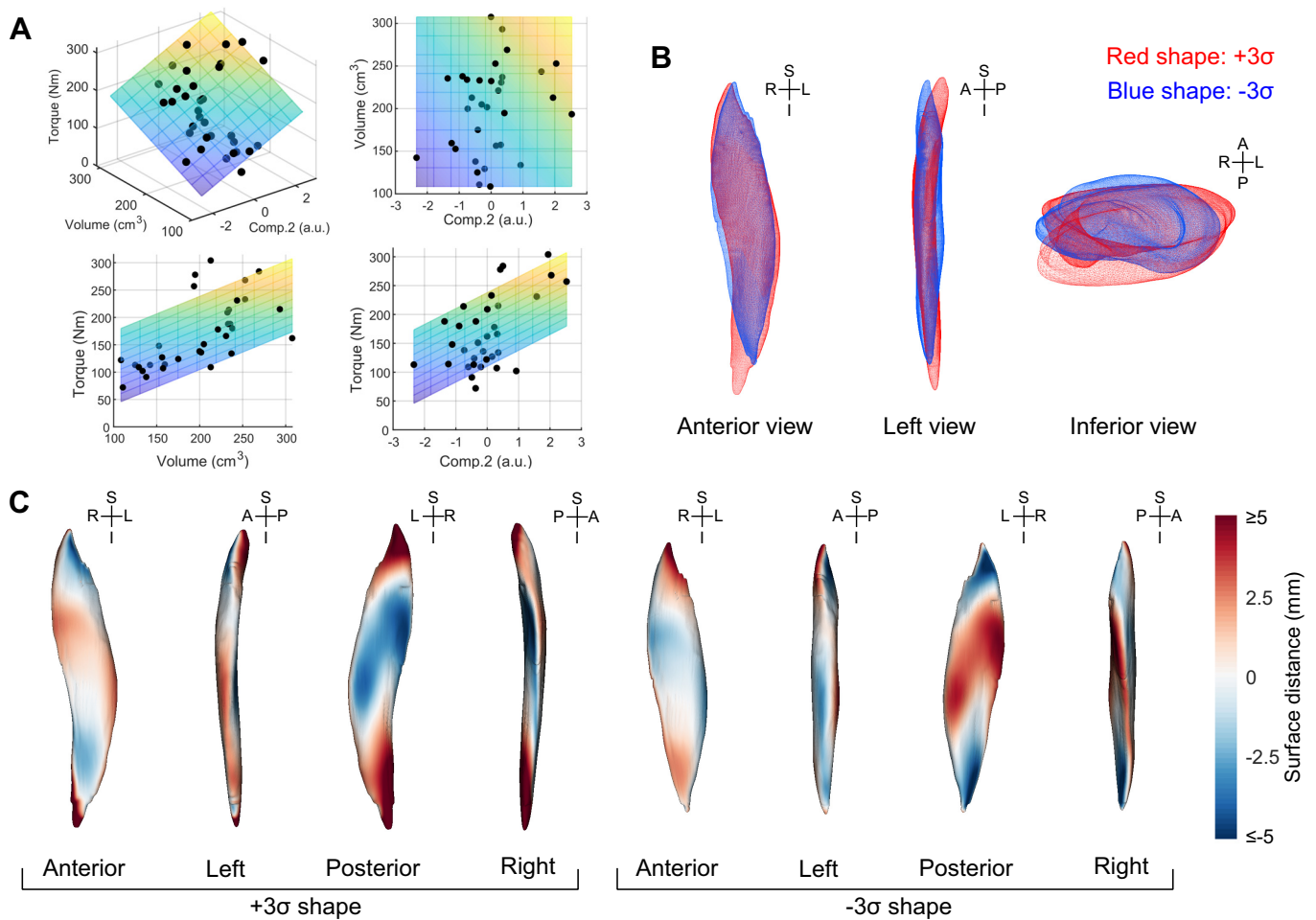


**Figure 5.** Muscle shape of rectus femoris (RF) relevant to muscle strength. **A:** relationship between muscle strength and muscle volume and shape. The dots represent individual data. The plane shows a least square plane fitted by the regression model to predict the knee extensor torque from the muscle volume and the *shape component 2*. **B:** shape comparison between +3 standard deviation ( $\sigma$ ) shape and  $-3\sigma$  shape. The red and blue shapes indicate the  $+3\sigma$  and  $-3\sigma$  shapes from mean shape, respectively. **C:** shape difference between mean shape and  $+3\sigma$  and  $-3\sigma$  shapes. The signed surface distance from the mean shape is visualized on the  $+3\sigma$  and  $-3\sigma$  shapes using color mapping. Red and blue indicate regions outside and inside the mean shape, respectively, and white represents a surface distance of zero. a.u., arbitrary unit.

were close to the perpendicular line with small variation (toward  $90^\circ$ ) (Muscle  $\times$  Plane:  $F = 4.0$ ,  $P < 0.001$ ,  $P_{\text{adj}} = 0.001$ ; Muscle:  $F = 2.0$ ,  $P = 0.120$ ,  $P_{\text{adj}} = 0.133$ ; Plane:  $F = 88.1$ ,  $P < 0.001$ ,  $P_{\text{adj}} < 0.001$ ).

Correlation analysis revealed the relationship between muscle shape and mechanical advantages (Fig. 8). The second shape component of RF tended to correlate with the flexion-extension moment arm in the sagittal plane ( $r = -0.32$ ,  $P = 0.065$ ,  $P_{\text{adj}} = 0.074$ ). The second shape component of VM significantly correlated with the spin moment arm in the coronal plane ( $\rho = 0.45$ ,  $P = 0.009$ ,  $P_{\text{adj}} = 0.014$ ). Therefore, the muscle shape with positive variance was associated with the increases in the RF extension moment arm and the VM large lateral spin moment arm. Besides, the second shape component was significantly related to the line-of-action of the coronal plane in RF ( $r = -0.42$ ,  $P = 0.015$ ,  $P_{\text{adj}} = 0.019$ ) and VM ( $\rho = -0.36$ ,  $P = 0.042$ ,  $P_{\text{adj}} < 0.050$ ). Consequently, the muscle shape with positive variance deviated the line-of-action from the perpendicular line, yielding a medial bias of their line-of-action within the coronal plane.

## DISCUSSION

Muscle morphology and its relationship to mechanical output are critical for understanding muscle function. Traditional methods, such as measuring muscle length and area, are inadequate for quantifying complex muscle morphology, leaving the impact of muscle shape on force generation capacity largely unexplored. Using statistical shape modeling, this study revealed that not only muscle volume but also the curvature and bulging of the RF and VM muscles significantly influence isometric knee extensor torque, whereas the volumes of the VL and VI contribute to torque, thereby partially supporting our hypothesis. This is the first study to demonstrate that skeletal muscle shape is a possible determinant of torque exertion.

In this research, we initially observed individual shape variations using the Jaccard similarity coefficient, with a mean value of  $\sim 0.74$  for all muscles. Although comparing this coefficient due to the lack of quantitative studies on muscle shape variation is challenging, the variation is relatively significant, as evidenced by the close correspondence

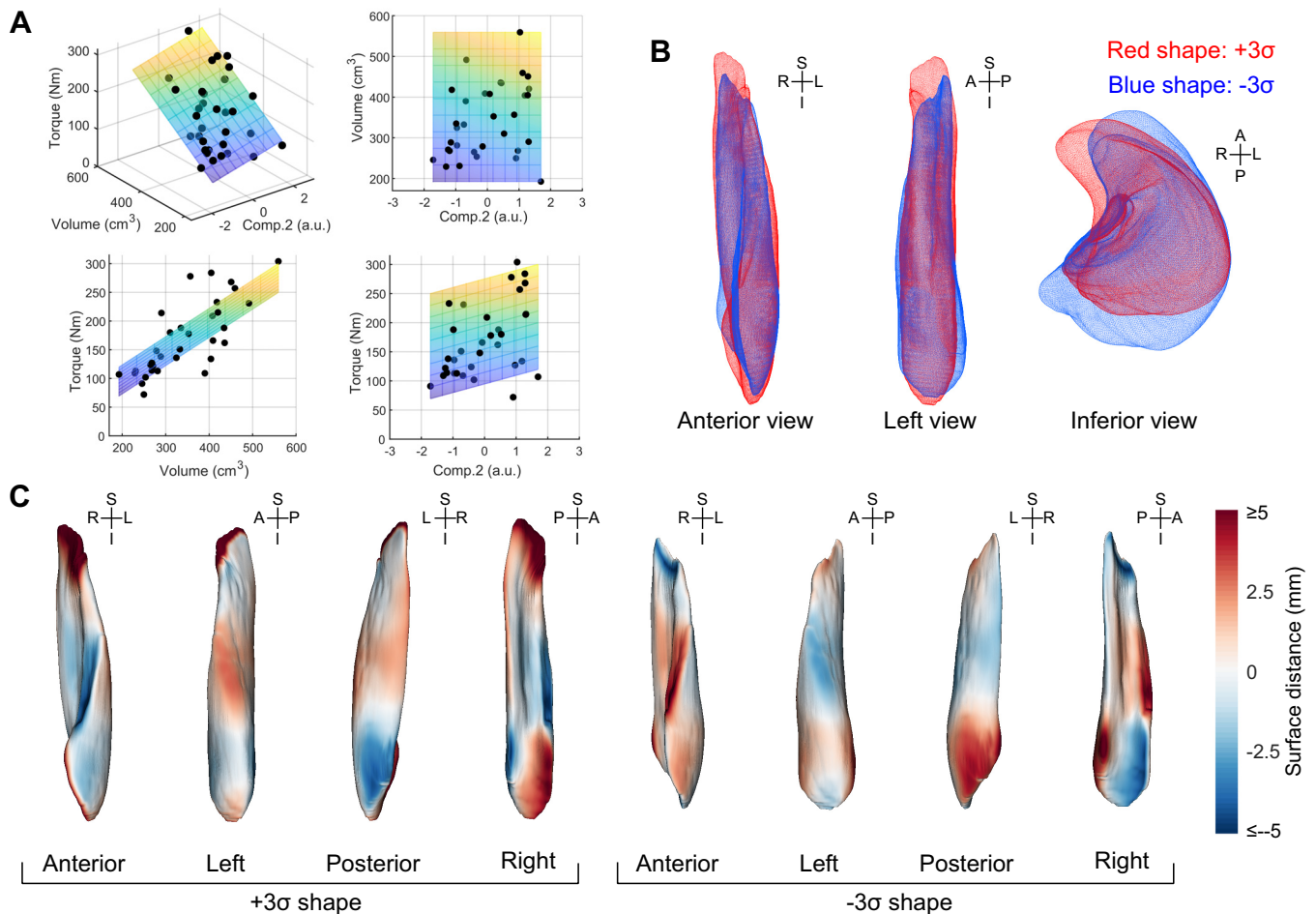


**Figure 6.** Muscle shape of vastus medialis (VM) relevant to muscle strength. A: relationship between muscle strength and muscle volume and shape. The dots represent individual data. The plane shows a least square plane fitted by the regression model to predict the knee extensor torque from the muscle volume and the *shape component 2*. The explanations for B and C are the same as those of Fig. 5. a.u., arbitrary unit.

of the mean Jaccard coefficient with the representatives of muscle shapes depicted in Supplemental Fig. S1. Notably, the shape variation was maintained even when the muscle geometry was normalized by muscle volume.

The statistical shape modeling is a promising method for quantifying the individual shape variation, though its application has been predominantly limited to skeletal muscle. To date, only two studies, to our knowledge, have applied this methodology to skeletal muscle. Bin Ghouth et al. (22) constructed the statistical shape model of the soleus muscle in cerebral palsy and typical developing children. Sutherland et al. (23) developed the statistical shape model of the hamstring muscle in rugby players and sprinters. Both studies found that the first component of the statistical shape model predominantly governed the size variation of the muscle. However, the second and subsequent components governed concave-convex, torsion, and curvature. This trend is consistent with our study in which the first shape component represented the size-dependent shape and governed large variations in length and width/thickness (66.3%–85.9%). The second and third components displayed curvature and bulging, indicating small variations (2.2%–4.6%). Size and shape covary, referred to as allometry (36), and size effect on shape

remain after size normalization (37). Indeed, a significant correlation between the first shape component and volume still existed in all muscles (correlation coefficients ranging from 0.79 to 0.85), even after volume scaling. Because the ratio of length to width/thickness is preserved after isovolume scaling, this size-dependent shape may represent the change in muscle shape along with maturation and hypertrophy/atrophy in young adults, which may be constrained in the musculoskeletal system (e.g., surrounding muscles, aponeuroses, and bones).

Our primary purpose was to investigate whether muscle shape impacts muscle strength. Significant correlations were observed between isometric knee extensor torque and the first shape component for all muscles. These relationships are obvious because the first component characterized the size-dependent shape of the muscle, such as length and width/thickness. Therefore, the first component represented the size of the anatomical/physiological cross-sectional area linked to the force generation capacity in skeletal muscle (1, 38). Of note, a significant correlation was observed between isometric knee extensor torque and the second shape component for the RF and VM muscles. The enlarged anteroposterior and mediolateral curvatures

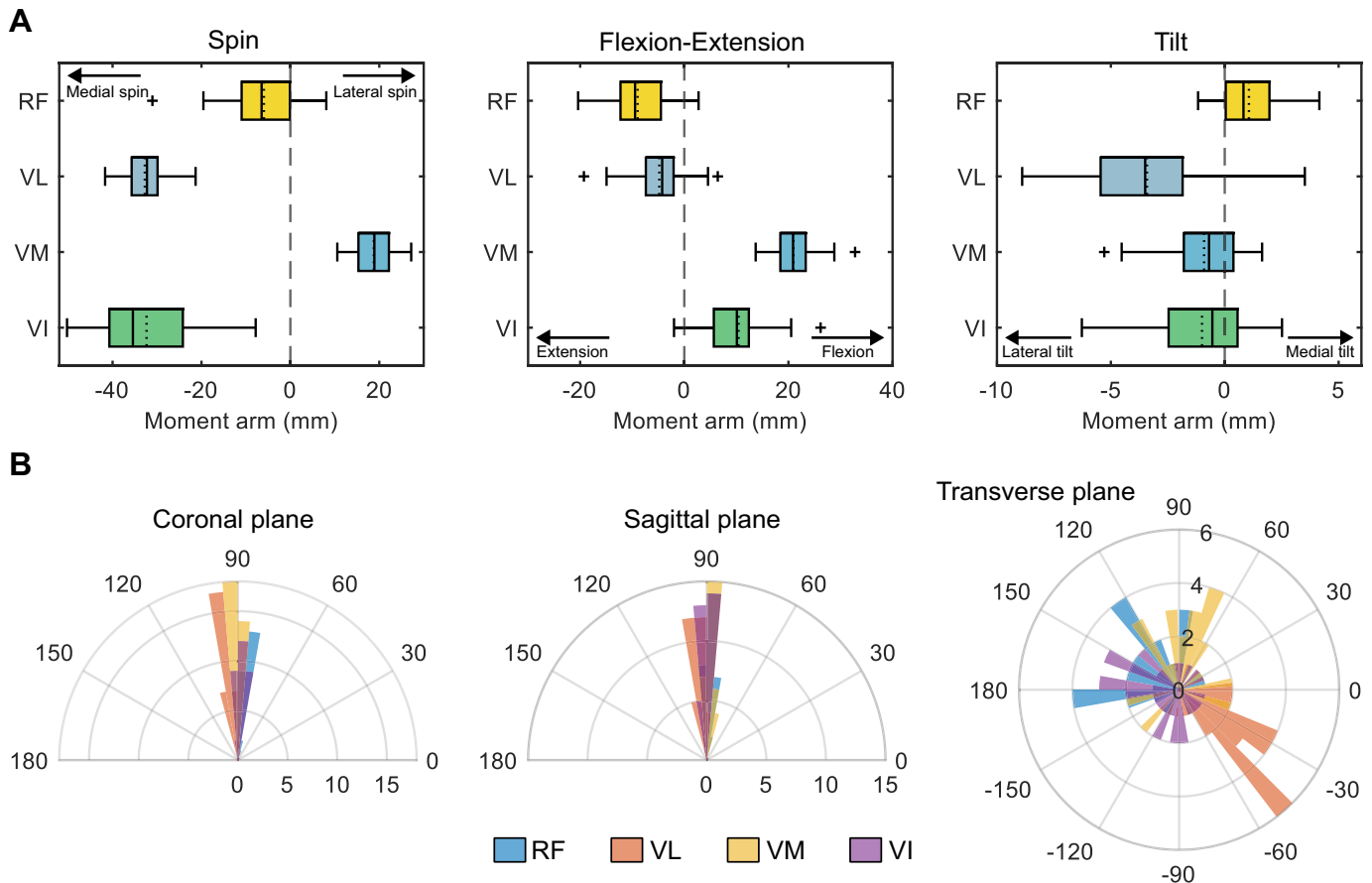


**Figure 7.** Mechanical advantages. *A*: the moment arms are displayed as lateral (+) and medial (-) spin (*left*), flexion (+) and extension (-) (*middle*), and medial (+) and lateral (-) tilt (*right*), shown in box and whisker plots. Vertical solid and dashed lines within the box indicate the medial and mean values, respectively. Whiskers indicate the first and third quartiles and the cross mark represents outlier. *B*: the lines of action are shown in a polar histogram. The lines of action are represented as a projection angle (degree) onto coronal (*left*), sagittal (*middle*), and transverse planes (*right*). The radius within the polar histogram indicates the number of participants at a given angle. RF, rectus femoris; VL, vastus lateralis; VM, vastus medialis; VI vastus intermedius.

of RF and the more pronounced bulging at the distal region of VM were associated with the increase in the magnitude of torque. Although correlation analysis observed size-related shape in VM, intriguingly, multiple regression analysis identified the shape features of RF and VM as determinants of knee extensor torque despite muscle volume, highlighting the significant contribution of muscle shape to joint torque output. To quantify the extent of muscle shape change, we calculated the surface distance, a quantitative measure of the shape difference, to determine the substantial differences in the muscle regions characterizing curvature and bulging (Figs. 5C and 6C). These muscle shapes were not attributable to methodological artifacts but morphological features (Supplemental Fig. S3). These findings provide the first direct evidence linking complex muscle shapes to mechanical output in skeletal muscle.

The rationale behind the muscle shape-torque relationship is noteworthy. Mechanical advantages may underlie this morphological functionality. This study therefore investigated the relationship between muscle shape and moment arm and line-of-action. The result revealed that the mechanical advantages follow the muscle shape. The second shape

component was positively correlated with the spin moment arm in VM. This relationship was comparable to that between its volume and spin moment arm ( $r = 0.47$ ), as examined in our post hoc analysis. The positive correlation of shape component and spin moment arm indicated that the muscle shape of more pronounced bulging in the distal region increased the moment arm of lateral spin. The lateral patellar spin was crucial in patellofemoral kinematics because the increase in medial patellar spin was related to the patellofemoral pain (33). In addition, the lateral patellar spin was positively correlated with the knee extension torque ( $\rho = 0.62$ ), as observed in our supplemental post hoc analysis. The VM was a unique muscle leveraging the moment arm of lateral spin, whereas the other vasti muscles exhibited the moment arm of medial spin. The VM with the lateral spin moment arm possibly contributed to regulating joint stress by generating resistance torque against the medial spin by other vasti muscles, yielding optimal torque production. Thus, the bulging of VM may influence the knee extension torque via the change in the patellar spin moment arm.

The muscle line-of-action could be another underlying mechanism governing the influence of shape on strength.

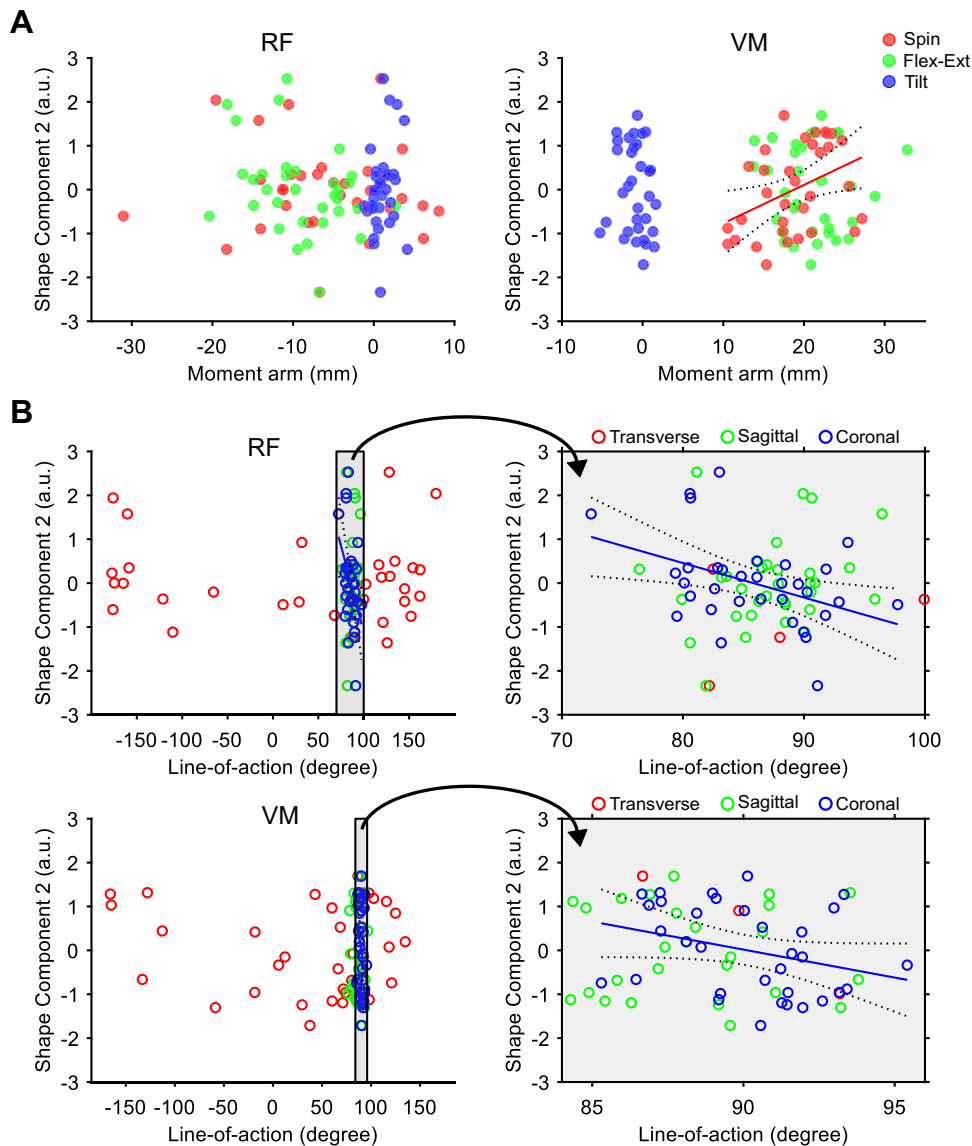


**Figure 8.** Relationship between muscle shape and mechanical advantages. *A*: correlation between *shape component 2* and moment arms in rectus femoris (RF) and vastus medialis (VM). The *shape component 2* is positively correlated with the spin moment arm in VM. *B*: correlation between *shape component 2* and lines of action in RF and VM. The *shape component 2* is negatively correlated with the line-of-action in coronal plane in both RF and VM. Solid line and dashed lines represent the linear regression line and 95% confidence interval estimated using the least-squares method. a.u., arbitrary unit.

The RF and VM second-shape components were significantly correlated with their line-of-action in the coronal plane, although this relationship was slightly weaker than that between volume and line-of-action in the coronal plane for the RF ( $r = -0.53$ ) and VM ( $r = -0.60$ ), as examined in our post hoc analysis. The negative correlation of shape component with line-of-action showed that the muscle shapes, particularly increased mediolateral curvature in RF and the more pronounced bulging in VM, influence the line-of-action toward the medial direction, generating the force pulling the patella medially. The knee extension torque was also negatively correlated with both the line-of-actions in the coronal plane for the RF ( $\rho = -0.52$ ) and VM ( $\rho = -0.55$ ), as observed in our supplemental post hoc analysis. The imbalance between medial and lateral forces suggested deviating from normal patellofemoral kinematics, leading to joint stress and pain (39, 40). In our study, the RF and VM muscles possessing the medial-directed line-of-action maintained the balance between medial and lateral forces, yielding efficient force transmission from the quadriceps femoris muscle to the knee

joint via the patella. Therefore, the curvature of RF and the bulging of VM may induce the change in line-of-action, influencing the torque production. After all, the muscle shape determined the mechanical advantages, optimizing output balance and influencing torque exertion.

Muscle shape does not necessarily reflect only moment arm and line-of-action. Force transmission and mechanical energy flow during contraction is another possible mechanism underlying the shape-related force output, although not evaluated in this study. Muscle is a composite and hierarchical structure, and muscle contraction is a three-dimensional process (41). Force transmission occurs between different structures and at different levels of organization and in directions both along the line-of-action and orthogonal to it (i.e., the radial direction) (42). Ultimately, a force component resulting from the transmission of force and the flow of mechanical energy within/between muscle(s) develops force output. In the context of muscle deformation and contraction dynamics, architectural gearing is highlighted as a mechanism for determining force

output (10). However, the outer shape of the muscle may operate as a constraint influencing force transmission and mechanical energy flow, thereby affecting force output. For instance, a curved shape may generate contact forces and affect energy transfer differently from a straight shape. The curvature of RF and bulging of VM may cause force transmission and mechanical energy flow favorable for output performance. Therefore, the muscle shape, formed by its specific features and its packing mechanism within the musculoskeletal system, may have functional implications and serve as a new proxy for muscle mechanical performance. This possibility is not analyzed in this study but could be investigated using an advanced 3-D muscle model with a finite element method (41, 43).

Muscle shape is not fixed but rather changes dynamically during contraction. The 3-D muscle shape during contraction best reflects the nature of contraction dynamics (42), although this was not measured in our study. The shapes of the VL and VI muscles at rest were not determinants of joint torque in our results. However, their contraction-induced shapes may be associated with torque exertion. Combining statistical shape modeling with dynamic MRI techniques (44) can elucidate muscle shape during contraction. However, the influence of 3-D muscle deformation during contraction on the mechanical output in human subjects requires further investigation.

When interpreting our results, several points should be noted. First, our participants were solely young, healthy adults. As muscle volume, intermuscular fat, and mechanical properties evolve with age (45, 46), muscle shape likely varies and affects the force-generating capacity in older adults, although this was not explored in this study. Second, we did not consider muscle architectures and mechanical properties in predicting joint torque. Integrating diffusion tensor imaging (47, 48) and MR- and ultrasound-elastography (49) with statistical shape modeling could enhance predictions of mechanical output. Third, the knee and hip joint configurations were different for MRI and torque measurements. This difference may deform muscle shape (50) and influence the results. Finally, our study focused only on the quadriceps femoris muscle. The quadriceps femoris comprises multiple synergist muscles for knee extension and may interact with them. Although it is a common experimental muscle and primary contributor to knee extension torque, studies are yet to determine whether similar results would be observed in other muscles.

In conclusion, this study determined whether the 3-D shape of the quadriceps femoris muscle influences isometric knee extensor torque by constructing a statistical shape model capable of quantifying the muscle morphology. Our findings indicate that knee extension torque is determined by both muscle volume and the shapes of the RF and VM through mechanical advantages, whereas the volumes of the VL and VI contribute to the torque. This study provides the first evidence of the impact of 3-D muscle shape on mechanical output and establishes a new framework for a better understanding of muscle morphology and its functional implications. In the future, biomechanics based on muscle shape may further advance our understanding of

human body function, athletic performance, and musculoskeletal disorders.

## APPENDIX

Bony landmarks were identified on the femur and patella to define the patella coordinate system. The origin was located in the contact point of the femur and patella. The mediolateral axis ( $y$ -axis) was defined as the unit vector from most lateral to medial points of the patella at the level of the patellofemoral contact point. The anteroposterior axis ( $x$ -axis) was defined as the unit vector normal to the plane containing the  $y$ -axis and a unit vector from the inferior pole to the superior pole of the patella. The vertical axis ( $z$ -axis) was the unit vector perpendicular to the  $x$ - and  $y$ -axes. The definition of a joint coordinate system was based on the previous studies with minor modifications (51).

## DATA AVAILABILITY

Raw data (MRI data) are available upon reasonable request from the corresponding author. Numerical data supporting the findings of this study are available from data repository: <https://doi.org/10.6084/m9.figshare.27940908>.

## SUPPLEMENTAL MATERIAL

Supplemental Figs. S1–S3: <https://doi.org/10.6084/m9.figshare.28511987>.

Supplemental Document: <https://doi.org/10.6084/m9.figshare.28512041>.

## ACKNOWLEDGMENTS

We thank Satoko Ibuki for the support of English writing, and all the members of the Clinical Biomechanics Laboratory of Kyoto University for constructive comments during research meetings. This study was conducted using the MRI scanner and related facilities of the Institute for the Future of Human Society, Kyoto University. This work was supported by the Strategic Project for Proofreading and Submission Support of International Academic Papers by Kansai Medical University.

## GRANTS

This work was supported by the Japan Society for the Promotion of Science (JSPS) KAKENHI Grant Number 21H03303 and 25K00132.

## DISCLOSURES

No conflicts of interest, financial or otherwise, are declared by the authors.

## AUTHOR CONTRIBUTIONS

J.U., M.T., and N.I. conceived and designed research; J.U., M.T., M. Yagi, Y.F., M. Yamagata, and R.N. performed experiments; J.U., G.L., and M.S. analyzed data; J.U., M.T., M. Yagi, M.S., Y.O., Y.S., and N.I. interpreted results of experiments; J.U. prepared figures; J.U. drafted manuscript; J.U., M.T., M. Yagi, and N.I. edited and revised manuscript; J.U., M.T., M. Yagi, G.L., M.S., Y.O., Y.S., Y.F., M. Yamagata, R.N., and N.I. approved final version of manuscript.

## REFERENCES

- Powell PL, Roy RR, Kanim P, Bello MA, Edgerton VR. Predictability of skeletal muscle tension from architectural determinations in guinea pig hindlimbs. *J Appl Physiol Respir Environ Exerc Physiol* 57: 1715–1721, 1984. doi:10.1152/jappl.1984.57.6.1715.
- Morse CI, Thom JM, Davis MG, Fox KR, Birch KM, Narici MV. Reduced plantarflexor specific torque in the elderly is associated with a lower activation capacity. *Eur J Appl Physiol* 92: 219–226, 2004. doi:10.1007/s00421-004-1056-y.
- Akagi R, Takai Y, Ohta M, Kanehisa H, Kawakami Y, Fukunaga T. Muscle volume compared to cross-sectional area is more appropriate for evaluating muscle strength in young and elderly individuals. *Age Ageing* 38: 564–569, 2009. doi:10.1093/ageing/afp122.
- Baxter JR, Piazza SJ. Plantar flexor moment arm and muscle volume predict torque-generating capacity in young men. *J Appl Physiol* (1985) 116: 538–544, 2014. doi:10.1152/japplphysiol.01140.2013.
- Fukunaga T, Miyatani M, Tachi M, Kouzaki M, Kawakami Y, Kanehisa H. Muscle volume is a major determinant of joint torque in humans. *Acta Physiol Scand* 172: 249–255, 2001. doi:10.1046/j.1365-201x.2001.00867.x.
- Blazevich AJ, Coleman DR, Horne S, Cannavan D. Anatomical predictors of maximum isometric and concentric knee extensor moment. *Eur J Appl Physiol* 105: 869–878, 2009. doi:10.1007/s00421-008-0972-7.
- Takahashi K, Kamibayashi K, Wakahara T. Gluteus and posterior thigh muscle sizes in sprinters: their distributions along muscle length. *Eur J Sport Sci* 22: 799–807, 2022. doi:10.1080/17461391.2021.1907450.
- Franchi MV, Atherton PJ, Reeves ND, Flück M, Williams J, Mitchell WK, Selby A, Beltran Valls RM, Narici MV. Architectural, functional and molecular responses to concentric and eccentric loading in human skeletal muscle. *Acta Physiol (Oxf)* 210: 642–654, 2014. doi:10.1111/apha.12225.
- Wakeling JM, Blake OM, Wong I, Rana M, Lee SS. Movement mechanics as a determinate of muscle structure, recruitment and coordination. *Philos Trans R Soc Lond B Biol Sci* 366: 1554–1564, 2011. doi:10.1098/rstb.2010.0294.
- Azizi E, Brainerd EL, Roberts TJ. Variable gearing in pennate muscles. *Proc Natl Acad Sci USA* 105: 1745–1750, 2008. doi:10.1073/pnas.0709212105.
- Randhawa A, Jackman ME, Wakeling JM. Muscle gearing during isotonic and isokinetic movements in the ankle plantarflexors. *Eur J Appl Physiol* 113: 437–447, 2013. doi:10.1007/s00421-012-2448-z.
- Dick TJM, Wakeling JM. Shifting gears: dynamic muscle shape changes and force-velocity behavior in the medial gastrocnemius. *J Appl Physiol* (1985) 123: 1433–1442, 2017. doi:10.1152/japplphysiol.01050.2016.
- Rockefeller R, Günther M, Clemente CJ, Dick TJM. Rethinking the physiological cross-sectional area of skeletal muscle reveals the mechanical advantage of pennation. *Roy Soc Open Sci* 11: 240037, 2024. doi:10.1098/rsos.240037.
- Heimann T, Meinzer HP. Statistical shape models for 3D medical image segmentation: a review. *Med Image Anal* 13: 543–563, 2009. doi:10.1016/j.media.2009.05.004.
- Ambellan F, Lamecker H, von Tycowicz C, Zachow S. Statistical shape models: understanding and mastering variation in anatomy. *Adv Exp Med Biol* 1156: 67–84, 2019. doi:10.1007/978-3-030-19385-0\_5.
- Dworzak J, Lamecker H, von Berg J, Klinder T, Lorenz C, Kainmüller D, Seim H, Hege H-C, Zachow S. 3D reconstruction of the human rib cage from 2D projection images using a statistical shape model. *Int J Comput Assist Radiol Surg* 5: 111–124, 2010. doi:10.1007/s11548-009-0390-2.
- Schneider MTY, Zhang J, Crisco JJ, Weiss AC, Ladd AL, Nielsen PMF, Besier T. Automatic segmentation of the thumb trapeziometacarpal joint using parametric statistical shape modelling and random forest regression voting. *Comput Methods Biomech Biomed Eng Imaging Vis* 7: 297–301, 2019. doi:10.1080/21681163.2018.1501765.
- Schneider MT, Rooks N, Besier T. Cartilage thickness and bone shape variations as a function of sex, height, body mass, and age in young adult knees. *Sci Rep* 12: 11707, 2022. doi:10.1038/s41598-022-15585-w.
- Schneider MT, Zhang J, Crisco JJ, Weiss AP, Ladd AL, Nielsen P, Besier T. Men and women have similarly shaped carpometacarpal joint bones. *J Biomech* 48: 3420–3426, 2015. doi:10.1016/j.jbiomech.2015.05.031.
- Saxby DJ, Killen BA, Pizzolato C, Carty CP, Diamond LE, Modenese L, Fernandez J, Davico G, Barzan M, Lenton G, da Luz SB, Suwarganda E, Devaprakash D, Korhonen RK, Alderson JA, Besier TF, Barrett RS, Lloyd DG. Machine learning methods to support personalized neuromusculoskeletal modelling. *Biomech Model Mechanobiol* 19: 1169–1185, 2020. doi:10.1007/s10237-020-01367-8.
- Fernandez J, Shim V, Schneider M, Choisne J, Handsfield G, Yeung T, Zhang J, Hunter P, Besier T. A narrative review of personalized musculoskeletal modeling using the physiome and musculoskeletal atlas projects. *J Appl Biomech* 39: 304–317, 2023. doi:10.1123/jab.2023-0079.
- Bin Ghouth SG, Williams SA, Reid SL, Besier TF, Handsfield GG. A statistical shape model of soleus muscle morphology in spastic cerebral palsy. *Sci Rep* 12: 7711, 2022. doi:10.1038/s41598-022-11611-z.
- Sutherland AMT, Lynch JT, Serpell BG, Pickering MR, Newman P, Perriman DM, Kenneally-Dabrowski C. Statistical shape modelling reveals differences in hamstring morphology between professional rugby players and sprinters. *J Sports Sci* 41: 164–171, 2023. doi:10.1080/02640414.2023.2204269.
- Li G, Otake Y, Soufi M, Taniguchi M, Yagi M, Ichihashi N, Uemura K, Takao M, Sugano N, Sato Y. Hybrid representation-enhanced sampling for Bayesian active learning in musculoskeletal segmentation of lower extremities. *Int J Comput Assist Radiol Surg* 19: 2177–2186, 2024. doi:10.1007/s11548-024-03065-7.
- Hiasa Y, Otake Y, Takao M, Ogawa T, Sugano N, Sato Y. Automated muscle segmentation from clinical CT using Bayesian U-net for personalized musculoskeletal modeling. *IEEE Trans Med Imaging* 39: 1030–1040, 2020. doi:10.1109/TMI.2019.2940555.
- Rueckert D, Sonoda LI, Hayes C, Hill DL, Leach MO, Hawkes DJ. Nonrigid registration using free-form deformations: application to breast MR images. *IEEE Trans Med Imaging* 18: 712–721, 1999. doi:10.1109/42.796284.
- de Jong S. SIMPLS: An alternative approach to partial least squares regression. *Chemom Intell Lab Syst* 18: 251–263, 1993. doi:10.1016/0169-7439(93)85002-X.
- Lekadir K, Hoogendoorn C, Pereanez M, Albà X, Pashaei A, Frangi AF. Statistical personalization of ventricular fiber orientation using shape predictors. *IEEE Trans Med Imaging* 33: 882–890, 2014. doi:10.1109/TMI.2013.2297333.
- Lee D, Li Z, Sohail QZ, Jackson K, Fiume E, Agur A. A three-dimensional approach to pennation angle estimation for human skeletal muscle. *Comput Methods Biomech Biomed Engin* 18: 1474–1484, 2015. doi:10.1080/10255842.2014.917294.
- Schache AG, Ackland DC, Fok L, Koulouris G, Pandy MG. Three-dimensional geometry of the human biceps femoris long head measured in vivo using magnetic resonance imaging. *Clin Biomech (Bristol)* 28: 278–284, 2013. doi:10.1016/j.clinbiomech.2012.12.010.
- Wilson NA, Sheehan FT. Dynamic in vivo quadriceps lines-of-action. *J Biomech* 43: 2106–2113, 2010. doi:10.1016/j.jbiomech.2010.04.002.
- Pandy MG. Moment arm of a muscle force. *Exerc Sport Sci Rev* 27: 79–118, 1999.
- Wilson NA, Sheehan FT. Dynamic in vivo 3-dimensional moment arms of the individual quadriceps components. *J Biomech* 42: 1891–1897, 2009. doi:10.1016/j.jbiomech.2009.05.011.
- Goparaju A, Iyer K, Bône A, Hu N, Henninger HB, Anderson AE, Durrleman S, Jaxsens M, Morris A, Csicsi I, Marrouche N, Elhabian SY. Benchmarking off-the-shelf statistical shape modeling tools in clinical applications. *Med Image Anal* 76: 102271, 2022. doi:10.1016/j.media.2021.102271.
- Li B, Morris J, Martin EB. Model selection for partial least squares regression. *Chemom Intell Lab Syst* 64: 79–89, 2002. doi:10.1016/S0169-7439(02)00051-5.
- Klingenberg CP. Heterochrony and allometry: the analysis of evolutionary change in ontogeny. *Biol Rev Camb Philos Soc* 73: 79–123, 1998. doi:10.1017/s000632319800512x.
- Lleonart J, Salat J, Torres GJ. Removing allometric effects of body size in morphological analysis. *J Theor Biol* 205: 85–93, 2000. doi:10.1006/jtbi.2000.2043.

38. **Jones EJ, Bishop PA, Woods AK, Green JM.** Cross-sectional area and muscular strength: a brief review. *Sports Med* 38: 987–994, 2008. doi:10.2165/00007256-200838120-00003.
39. **Besier TF, Fredericson M, Gold GE, Beaupré GS, Delp SL.** Knee muscle forces during walking and running in patellofemoral pain patients and pain-free controls. *J Biomech* 42: 898–905, 2009. doi:10.1016/j.jbiomech.2009.01.032.
40. **Hug F, Tucker K.** Muscle coordination and the development of musculoskeletal disorders. *Exerc Sport Sci Rev* 45: 201–208, 2017. doi:10.1249/JES.0000000000000122.
41. **Wakeling JM, Ross SA, Ryan DS, Bolsterlee B, Konno R, Domínguez S, Nigam N.** The energy of muscle contraction. I. Tissue force and deformation during fixed-end contractions. *Front Physiol* 11: 813, 2020. doi:10.3389/fphys.2020.00813.
42. **Roberts TJ, Eng CM, Sleboda DA, Holt NC, Brainerd EL, Stover KK, Marsh RL, Azizi E.** The multi-scale, three-dimensional nature of skeletal muscle contraction. *Physiology (Bethesda)* 34: 402–408, 2019. doi:10.1152/physiol.00023.2019.
43. **Bolsterlee B, Lloyd R, Bilston LE, Herbert RD.** A mechanically consistent muscle model shows that the maximum force-generating capacity of muscles is influenced by optimal fascicle length and muscle shape. *J Biomech* 182: 112584, 2025. doi:10.1016/j.jbiomech.2025.112584.
44. **Hooijmans MT, Schlaffke L, Bolsterlee B, Schlaeger S, Marty B, Mazzoli V.** Compositional and functional MRI of skeletal muscle: a review. *J Magn Reson Imaging* 60: 860–877, 2024. doi:10.1002/jmri.29091.
45. **Morse CI, Thom JM, Reeves ND, Birch KM, Narici MV.** In vivo physiological cross-sectional area and specific force are reduced in the gastrocnemius of elderly men. *J Appl Physiol (1985)* 99: 1050–1055, 2005. doi:10.1152/jappphysiol.01186.2004.
46. **Pinel S, Kelp NY, Bugeja JM, Bolsterlee B, Hug F, Dick TJM.** Quantity versus quality: Age-related differences in muscle volume, intramuscular fat, and mechanical properties in the triceps surae. *Exp Gerontol* 156: 111594, 2021. doi:10.1016/j.exger.2021.111594.
47. **Bolsterlee B.** A new framework for analysis of three-dimensional shape and architecture of human skeletal muscles from in vivo imaging data. *J Appl Physiol (1985)* 132: 712–725, 2022. doi:10.1152/jappphysiol.00638.2021.
48. **Takahashi K, Shiotani H, Evangelidis PE, Sado N, Kawakami Y.** Three-dimensional architecture of human medial gastrocnemius fascicles in vivo: Regional variation and its dependence on muscle size. *J Anat* 241: 1324–1335, 2022. doi:10.1111/joa.13750.
49. **Dick TJM, Hug F.** Advances in imaging for assessing the design and mechanics of skeletal muscle in vivo. *J Biomech* 155: 111640, 2023. doi:10.1016/j.jbiomech.2023.111640.
50. **Bolsterlee B, D'Souza A, Gandevia SC, Herbert RD.** How does passive lengthening change the architecture of the human medial gastrocnemius muscle? *J Appl Physiol (1985)* 122: 727–738, 2017. doi:10.1152/jappphysiol.00976.2016.
51. **Seisler AR, Sheehan FT.** Normative three-dimensional patellofemoral and tibiofemoral kinematics: a dynamic, in vivo study. *IEEE Trans Biomed Eng* 54: 1333–1341, 2007. doi:10.1109/TBME.2007.890735.